

Accepted Manuscript

Research paper

A series of three isostructural 1D lanthanide coordination network based on 4,4',4''-((benzene-1,3,5-triyltris(methylene))tris(oxy))tribenzoate ligand: Synthesis, crystal structure and photophysical properties

Lanousse Petiote, Filipe M. Cabral, André L.B. Formiga, Italo O. Mazali, Fernando A. Sigoli

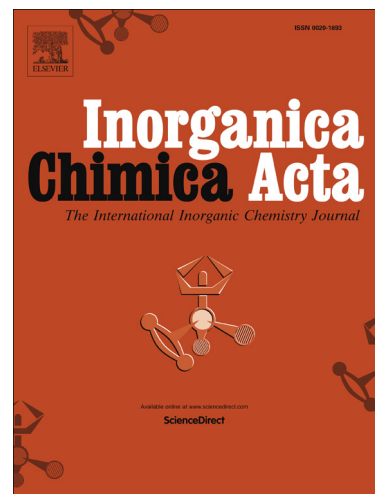
PII: S0020-1693(19)30102-1
DOI: <https://doi.org/10.1016/j.ica.2019.05.005>
Reference: ICA 18906

To appear in: *Inorganica Chimica Acta*

Received Date: 19 January 2019
Revised Date: 17 March 2019
Accepted Date: 2 May 2019

Please cite this article as: L. Petiote, F.M. Cabral, A.L.B. Formiga, I.O. Mazali, F.A. Sigoli, A series of three isostructural 1D lanthanide coordination network based on 4,4',4''-((benzene-1,3,5-triyltris(methylene))tris(oxy))tribenzoate ligand: Synthesis, crystal structure and photophysical properties, *Inorganica Chimica Acta* (2019), doi: <https://doi.org/10.1016/j.ica.2019.05.005>

This is a PDF file of an unedited manuscript that has been accepted for publication. As a service to our customers we are providing this early version of the manuscript. The manuscript will undergo copyediting, typesetting, and review of the resulting proof before it is published in its final form. Please note that during the production process errors may be discovered which could affect the content, and all legal disclaimers that apply to the journal pertain.



A series of three isostructural 1D lanthanide coordination network based on 4,4',4''-((benzene-1,3,5-triyltris(methylene))tris(oxy))tribenzoate ligand: Synthesis, crystal structure and photophysical properties

Lanousse Petiote, Filipe M. Cabral, André L. B. Formiga, Italo O. Mazali, Fernando A. Sigoli*

Laboratory of Functional Materials, Department of Inorganic Chemistry, Institute of Chemistry, UNICAMP, Campinas, 13083-970, Brazil

*fsigoli@unicamp.br

Abstract

Three 1D-coordination networks namely $\{[\text{Ln}(\text{L})(\text{DMF})(\text{H}_2\text{O})]\cdot\text{DMF}\}_n$ represented as EuL, GdL and TbL were obtained using the synthesized 4,4',4''-((benzene-1,3,5-triyltris(methylene))tris(oxy))tribenzoic acid (H_3L) as a ligand and lanthanide nitrate salts ($\text{Ln}(\text{NO}_3)_3$) ($\text{Ln} = \text{Eu}^{\text{III}}$, Gd^{III} or Tb^{III}). The reactions were carried out under solvothermal conditions using a mixture of DMF and H_2O . Single crystal X-ray analyses revealed that all three compounds are isostructural crystalizing in the triclinic space group $P\bar{1}$. They show an interesting binodal connected one-dimensional structure, with a static crystal disorder due to the different spatial orientations of DMF molecules. The triplet state energy of the H_3L ligand obtained from $\{[\text{Gd}(\text{L})(\text{DMF})(\text{H}_2\text{O})]\cdot\text{DMF}\}_n$ lies energetically above the main emitting states of both Eu^{III} and Tb^{III} . The photophysical properties were investigated in terms of excitation, emission spectra and emission lifetime at three different temperatures. EuL and TbL exhibit characteristic emission bands of the Eu^{III} and Tb^{III} with emission lifetimes of 0.51 ms and 0.90 ms, respectively. The emission lifetime values of EuL and TbL remain practically constant in the temperature range from 77 to 300 K. Furthermore, it is mentioned a possible effect of a crystal disorder on the luminescence profile of Eu^{III} in EuL.

Keywords

Lanthanide coordination network, single crystal, photoluminescence 4,4',4''-((Benzene-1,3,5-triyltris(methylene))tris(oxy))tribenzoic acid.

Introduction

The luminescent properties of lanthanide-based coordination networks (Ln-CPs) have attracted considerable interest in the supramolecular chemistry and crystal engineering not only due to their diverse topologies and intriguing structures but also owing to their unique photophysical properties resulting from the $4f^n$ electronic configurations of the trivalent ions [1–3]. This class of compounds combine the intrinsic characteristics of the metal organic framework [4] with the peculiar photophysical properties of the trivalent lanthanide (Ln^{III}) ions including reasonable luminescence quantum yield, narrow emission band and long emission lifetimes [5]. These characteristics make them potential candidates for applications in many fields such as: lighting devices [6], optical communications, chemical sensing [7], photonics and biomedical devices [8]. Furthermore, lanthanide coordination networks have been investigated in gas storage and separation [9], proton conductivity [10], catalysis [11] and molecular magnetism [12] exploring magneto-luminescent bimodal systems [13]. As some examples of the latter application, Huang et al. reported weak $\text{Tb}^{\text{III}}\text{--Tb}^{\text{III}}$ ferromagnetic interactions in $[\text{Tb}_2(\text{tdc})_3(\text{H}_2\text{O})_4]$ (tdc = thiophene-2,5-dicarboxylate di-anions) and Tb^{III} typical luminescence [14]. Ferromagnetic coupling between trivalent lanthanides centers in $[\text{Er}(\text{pza})(\text{OH})(\text{H}_2\text{O})]$ and $[\text{Dy}(\text{cit})(\text{H}_2\text{O})_n]$ (cit = citrate tri-anions) was reported by Weng and Li, respectively [14,15]. More recently, Kumar and co-authors reported interesting magnetic properties owing from $\text{Dy}^{\text{III}}\text{--Dy}^{\text{III}}$ and $\text{Er}^{\text{III}}\text{--Er}^{\text{III}}$ interactions in two 3D coordination polymers constructed from the ligands 3,5-pyridinedicarboxylic and adipic acids [16]. Using the thiophene-2,5-dicarboxylate as main building ligand. Mohd Yawer and co-authors also reported antiferromagnetic interactions between lanthanide ions in 3D metal organic frameworks [17]. Trivalent lanthanide ions form complexes with variable coordination numbers and geometries that may influence their photophysical properties [18]. Among trivalent lanthanides, Eu^{III} and Tb^{III} ions are the most used as optical centers in the visible range due their pure-color emissions owing from the $^5\text{D}_0 \rightarrow ^7\text{F}_J$ ($J = 0\text{--}4$) and $^5\text{D}_4 \rightarrow ^7\text{F}_J$ ($J = 6\text{--}3$) electronic transitions [19], respectively. Additionally, lanthanide based networks containing Tb^{III} and Eu^{III} are suitable for

development of ratiometric thermal optical probes for luminescence based thermometry [20] and chemical sensing [21]. Using the Eu-CP [Eu(pdc)_{1.5}(DMF)]·(DMF)_{0.5}(H₂O)_{0.5} (pdc = pyridine-3,5-dicarboxylate), Chen and co-authors reported the detection of Cu^{II} in a DMF solution. The weak binding of the pyridyl nitrogen to the d-metal ion reduces the energy transfer efficiency from the pdc ligand to Eu^{III} leading to its luminescence quenching [3]. The same group pioneered the use of lanthanide coordination networks for sensing in biological systems [22] using the Ln-CP Eu₂(FMA)₂(OX)(H₂O)₄ where FMA = fumarate and OX = oxalate [23]. Subsequently, many works were reported about optical sensing. Luo and co-authors exploited the Eu^{III}-doped coordination polymer [NH₄]_{0.7}[Eu][ZnL][Cl]_{1.7}(H₂O)₈ (L = 1,2,4,5-benzenetetracarboxylate) for Cu^{II} sensing in aqueous solution [24]. Song and co-authors reported the Eu^{III}-CP based on the tetrakis[4-(carboxyphenyl)oxamethyl]methane acid tetrakis[4-(carboxy phenyl) oxamethyl]methane acid) with potential for Fe^{III} sensing [25].

Due to the Laporte forbidden nature of the f-f electronic transitions, the trivalent lanthanides have very small molar absorptivity, less than 10 L⁻¹ mol⁻¹ cm⁻¹ [26], resulting in weak photoluminescence upon direct excitation [19]. To overcome this limitation, the organic ligand takes a decisive role. The Ln-CP building normally incorporate strong absorbing groups which will sensitize, via the antennae effect [27], the trivalent lanthanide luminescence [21]. As it is well known, organic ligand with suitable singlet and triplet energies may significantly enhance lanthanide trivalent luminescence [28]. In specific cases of Eu^{III} and Tb^{III} ions, the organic ligand must have an appropriate energy of the triplet state in the range of 22000 to 27000 cm⁻¹ to match the main accepting energy levels of Tb^{III} (⁵D₄: 20500 cm⁻¹) and Eu^{III} (⁵D₁:19030 cm⁻¹) [5,29]. Considering the oxophilicity of the trivalent lanthanide ions [30], one strategy for CP building consist in using polydentate aromatic carboxylic acids which can strongly bound to the metal ion in a versatile coordination modes [31,32], offering several types of coordination [29] polyhedral geometries, and at the same time act as chromophoric moieties for luminescence sensitization [33]. In this work the ligand, 4,4',4''-((Benzene-1,3,5-triyltris(methylene))tris-(oxy))tribenzoic acid (H₃L) (ESI Scheme S1) was synthesized and subsequently used to prepare three Ln-CPs (Ln = Eu, Gd, Tb). The H₃L ligand contains three carboxylate and

four phenyl groups being promising for versatile coordination mode and sensitizing the luminescence of both Eu^{III} and Tb^{III} ions. The three compounds namely EuL, GdL and TbL were obtained via solvothermal approach using an DMF / water mixing solvents and they were structurally characterized by single crystal and powder X-ray diffractions, TG, FT-IR, UV-Vis spectroscopy and their photophysical properties were investigated in terms of photoluminescence spectra and emission lifetimes.

2. Experimental section

2.1 Materials and methods.

The ligand 4,4',4''-((benzene-1,3,5-triyltris(methylene))tris(oxy))tribenzoic acid was prepared by a one pot synthesis as further described. Aqueous solutions of lanthanide nitrate salts (pH ~6) were prepared dissolving lanthanide oxide in concentrated nitric acid. All other reagents and solvents were purchased and used as received without further purification. The solvothermal reactions were performed in a 40 mL Teflon-lined stainless-steel autoclave under autogenous pressure. ¹H nuclear magnetic resonance (¹H-NMR) spectrum was collected on a Bruker AVANCE 400 spectrometer. Single-crystal X-ray diffraction data were collected on a Bruker Apex Duo diffractometer equipped with a graphite-monochromatized Mo K α radiation ($\lambda = 0.71073 \text{ \AA}$) at 150 K. All structures were solved and refined by direct methods with full-matrix least-squares refinements based on F^2 using SHELXS-97 and SHELXL-97 program packages [34]. All non-hydrogen atoms were refined anisotropically and hydrogen atoms were placed in geometrically calculated positions. The R_1 and wR_2 values are defined as $R_1 = \sum(|F_0| - |F_c|) / \sum|F_0|$ and $wR_2 = \left\{ \frac{\sum[w(F_0^2 - F_c^2)^2]}{\sum[w(F_0^2)^2]} \right\}^{1/2}$, respectively. CCDC 1875767 (TbL), CCDC 1875768 (EuL) and CCDC 1875769 (GdL) contain the crystallographic data in CIF format. Calculated P-XRD were obtained by using the Mercury program [35]. To determine the crystalline phase of the samples obtained as a microcrystalline powder together with monocrystals of the Ln-CPs, P-XRD measurements were performed on a Bruker D8 ADVANCE X-ray powder diffractometer using a Cu- α radiation (1.5418 \AA) at room temperature with 2θ ranging from 5° to 50°. Thermogravimetric analyses were conducted under synthetic air on a Universal V2.6 DTA system by heating

up from 30 to 900 °C with a heating rate of 10 °C min⁻¹. FT-IR spectra were recorded using an Agilent FT-IR spectrometer (CARY 630) in ATR mode using a diamond crystal in the range of 4000–400 cm⁻¹. Elemental analyses (C, H, N) were determined using an elemental analyzer Perkin Elmer (CHN 2400). The photoluminescence data were obtained on a Fluorolog-3 spectrofluorometer (Horiba FL3-22-iHR320), with double-gratings (1200 g mm⁻¹, 330 nm blaze) in the excitation monochromator and double-gratings (1200 g mm⁻¹, 500 nm blaze) in the emission monochromator. An ozone-free xenon lamp of 450 W (Ushio) was used as the radiation source. The excitation spectra were corrected in real time according to the lamp intensity and the optical system of the excitation monochromator using a silicon diode as reference. The emission spectra were recorded using the front face mode at 22.51°. All of them were corrected according to the optical system of the emission monochromator and the photomultiplier response (Hamamatsu R928P). Time-resolved phosphorescence emission spectra of the analogous Gd^{III} compound (GdL) were obtained at ~77 K using a time-correlated single photon counting (TCSPC) system, in order to get only emission bands from triplet levels of the ligand. The emission decay curves were obtained with a flash 150 W xenon lamp using the same TCSPC accessory.

2.2 Synthesis of H₃L

A mixture of 1,3,5-tris(bromomethyl)benzene (1.5 g; 4.2 mmol), ethyl 4-hydroxybenzoate (2.1 g, 12.6 mmol), sodium carbonate (2.0 g, 18.9 mmol) in dimethylformamide (DMF) (20 mL) was carried out in a single neck round bottom flask and magnetically stirred at 80 °C for 72 h. After cooling to room temperature, the solvent was removed at 60 °C by vacuum assisted rotary evaporation to obtain a white powder that was subsequently suspended in acetone (20 mL) and combined with NaOH (1.0 g) dissolved in water (20 mL). This mixture was stirred at 80 °C for 24 h. After cooling to room temperature, the acetone fraction was eliminated by vacuum assisted evaporation at 50 °C and the resulting aqueous solution was acidified (pH~1) by addition concentrated hydrochloric acid dropwise resulting in a yellow gelatinous precipitate which was collected by vacuum filtration and washed with water until pH=4-5. The crystallized powder was obtained by dissolving the product in

acetone and using water as poor solvent. After drying, 1.85 g (yield = 83%) of the protonated ligand was isolated as a yellow powder. $^1\text{H-NMR}$ (400 MHz, DMSO): δ / ppm = 5.23 (s, 6 H, CH₂), 7.13 (d, $J_{\text{HH}} = 8.9$ Hz, 6 H, Ar-H), 7.55 (s, 3 H, Ar-H), 7.90 (d, $J_{\text{HH}} = 8.9$ Hz, 6 H, Ar-H), 12.66 (s, 3 H, COOH). Elemental analysis (%) - found (calculated) for C₃₀H₂₄O₉ C = 68.10 (68.18); H = 4.60 (4.58).

2.3 Synthesis of the coordination networks

Three syntheses were carried out following a solvothermal method [36] as follow: 60.0 mg (0.14 mmol) of 4,4',4''-((benzene-1,3,5-triyltris(methylene))-tris(oxy))tribenzoic acid (H₃L) was dissolved in 10 mL of DMF in the 40 mL Teflon-lined stainless-steel vessel. Then 100 μL of concentrated HCl and 0.14 mol of Ln(NO₃)₃ in 2 mL of water were added sequentially. After sealed, the reaction mixture was heated at 120°C for 72 hours. After cooling down to room temperature, the resulting yellow crystals were washed using DMF and water and dried in reduced pressure at 50°C yielding ca. 50 % based on the lanthanide ions. {[Eu₂(L)₂(DMF)₂(H₂O)₂].DMF}_n. (EuL). Yield 54 %. Elemental analysis (%) - found (calcd) for Eu₂C₆₉H₆₇N₃O₂₃ (MW = 1610.22 g.mol⁻¹), C = 51.10 (51.47); H = 4.23 (4.19); N = 2.65 (2.61). {[Gd₂(L)₂(DMF)₂(H₂O)₂].DMF}_n. (GdL). Yield 55 %. Elemental analysis (%) - found (calcd) for Gd₂C₆₉H₆₇N₃O₂₃ (MW = 1620.79 g mol⁻¹), C = 51.10 (51.13); H = 4.27 (4.17); N = 2.61 (2.59). {[Tb₂(L)₂(DMF)₂(H₂O)₂].DMF}_n (TbL) Yield 49 %. Elemental analysis (%) - found (calcd) for Tb₂C₆₉H₆₇N₃O₂₃ (MW = 1624.14 g.mol⁻¹), C = 50.89 (51.03); H = 4.20 (4.16); N = 2.62 (2.59).

3. Results and discussion

3.1 Synthesis and characterization of the ligand 4,4',4''-((benzene-1,3,5-triyltris(methylene))-tris(oxy))tribenzoic acid (H₃L)

The ligand 4,4',4''-((benzene-1,3,5-triyltris(methylene))tris(oxy))tribenzoic acid (H₃L) was prepared using a one pot synthesis based on a modified reported procedure [37]. The scheme of the synthesis is shown on electronic supporting information (ESI Scheme S2). Firstly, the tri-ester (ESI Scheme S2 - III) was obtained by reaction of 1,3,5- tris(bromomethyl)benzene (ESI Scheme S2 - II) with ethyl 4-hydroxybenzoate (ESI Scheme S2 - I) in the presence of

sodium carbonate DMF for 72 hours. After the reaction time, the solvent was removed, and the white crude precipitate was dissolved in the mixture of acetone and aqueous solution of NaOH to obtain the ligand as his sodium salt (ESI Scheme S2 - IV) after 24 hours. It is noteworthy that the use of the mixture of solvents was important to guarantee that the reaction was carried out in the liquid state, once the ester is not water-soluble. After elimination of the acetone, concentrated chloride acid was added to precipitate the acid (ESI Scheme S2 - V), which was isolated, washed and dried to yield 83 % of the expected mass.

As can be seen in Fig. 1, single crystals were obtained on slow water diffusion into a diluted solution of the ligand in DMF. As reported by Sebastian et. al. [37], the as-synthesized ligand crystalizes in the triclinic space $P\bar{1}$ with a asymmetric unit consisting in one molecule (Fig. 1). Its molecular geometry differs completely from the trigonal one. Two of the molecular branches are arranged in a pincer-like fashion stabilized by an intra-molecular π - π interaction between two aromatic rings that are 4.013 Å apart. The third molecular arm is oriented in the opposite direction conferring an elongated conformation of the molecule in the crystal. Crystallographic data, experimental parameters and selected details of the refinements are summarized in Table 1.



Fig. 1: Ball illustration of the molecular structure of the ligand 4,4',4''-((Benzene-1,3,5-triyltris(methylene))tris(oxy))tribenzoic Acid (H_3L). The dark dots and the dotted-line between aromatic rings represent the centroids and distance between them, respectively.

The 1H -NMR spectrum (Figure S1) suggests that the ligand was obtained in high purity corroborating the elemental analysis result. Its UV-Vis electronic spectrum in acetonitrile solution (Figure S4) shows two absorption bands centered at 253 nm and at ca. 200 nm which may be assigned to ($\pi^* \leftarrow n$) involving non-bonding electron pairs of the oxygen atoms and ($\pi^* \leftarrow \pi$)

electronic transitions in the aromatic rings, respectively. Using the single crystal molecular structure, a TD-DFT calculation was performed to estimate the first excited state of the free ligand. Firstly, the hydrogen atoms were optimized by DFT calculations using PBE0 [38,39] functional and the basis def2-TZVP [40,41] in the Orca 4.0.1 [42] software. Using the optimized structure, the TD-DFT calculations were performed to estimate the energy of excited states. As can be seen in Figure S4, the calculated absorption spectrum of the free ligand agrees with the experimental spectrum obtained experimentally in a dilute acetonitrile solution.

3.2 Syntheses and characterization of the coordination networks.

Solvothermal conditions have been proven to be a useful methodology to obtain crystalline coordination networks. As the ligand is soluble in DMF, the chloridric acid was used to reduce the coordination speed and consequently potentialize growth of high-quality single crystals [43]. As the acid slows down the deprotonation of the carboxylate group and consequently, the binding of the linkers to the metal centers, it promotes growth of larger crystals and prevents formation of amorphous and polycrystalline phases, which may be formed if the reaction is allowed to proceed with no acid added [26]. X-ray single crystal structure analyses reveal that the three synthesized compounds EuL, GdL, TbL are isostructural (see Table1) and simulated powder X-ray diffraction pattern (Figure S8) crystallizing in the triclinic space group crystal system $P\bar{1}$ and feature an extended isolated 1D structure. Thus, the representative structure description and discussion will be restricted to the Eu^{III} compound EuL. As can be seen in Fig. 2, the asymmetric unit of EuL contains one Eu^{III} ion, one totally deprotonated ligand L, one DMF and one water molecule coordinated to the metal center and one lattice DMF molecule. Each europium ion is eight-coordinated and binds two oxygen atoms from one DMF and one H_2O molecule (average bond length of 2.415 and 3.093 Å, respectively) and carboxylate oxygen atoms belonging to three different L^{3-} tri-anions that coordinate to the metal ion in the bridging and the chelating bis-dentate modes (average Eu-O bond length of 2.292 and 2.461 Å, respectively). The coordination geometry of the Eu^{III} ion (Fig. 3) can be viewed as a distorted square antiprism, where the basal planes is formed by O4, O5, O6, O10, and O7, O8, O9 O11 atoms,

respectively, leading to a C_1 point group, therefore a low-symmetry coordination sphere without inversion center around the metal center. Each ligand L^{3-} binds to three metal ions through two chelating and one bidentate carboxylate groups (Figure S2). Two non-centrosymmetric Eu atoms bridged through the same carboxylate group generate a binuclear $Eu_2(\mu_2-COO)_2$ unit where the distance between the metal ions is 4.816 Å (Fig. 4). The binuclear units are linked along the b axis in the infinite 1D chains (Fig. 5), which are further packed in a 3D network (Fig. 6). Each dinuclear unit is surrounded by four L^{3-} ligands (Figure S3) and each ligand connects to two binuclear units, the 1D chain of EuL is defined as a 2,4-connected network.

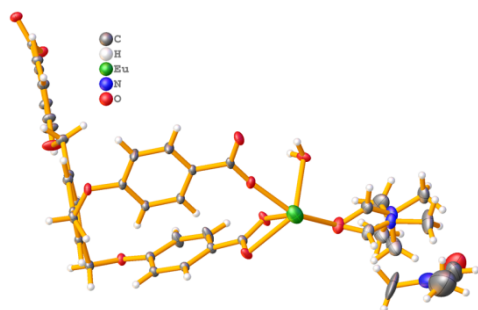


Fig. 2: Ball drawing of the asymmetric unit of EuL .

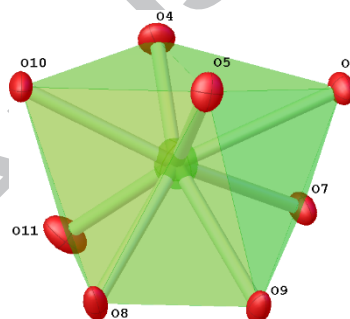


Fig. 3: The coordination geometries of Eu^{III} ions in EuL resulting in a C_1 site for the central ion.

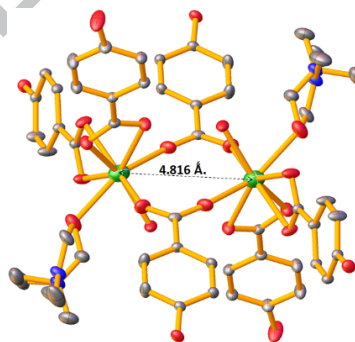


Fig. 4: The connection mode of Eu^{III} ions in a binuclear unit.

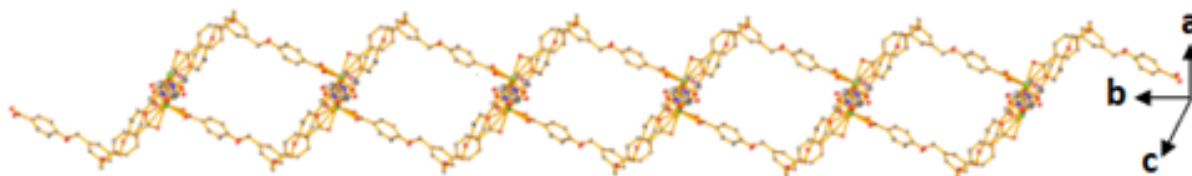


Fig. 5: View of the 1D chain as the infinite secondary building units (SBUs) along the crystallographic b-axis obtained from binuclear units linked through carboxylate group. H atoms and free solvent molecules were omitted for clarity.

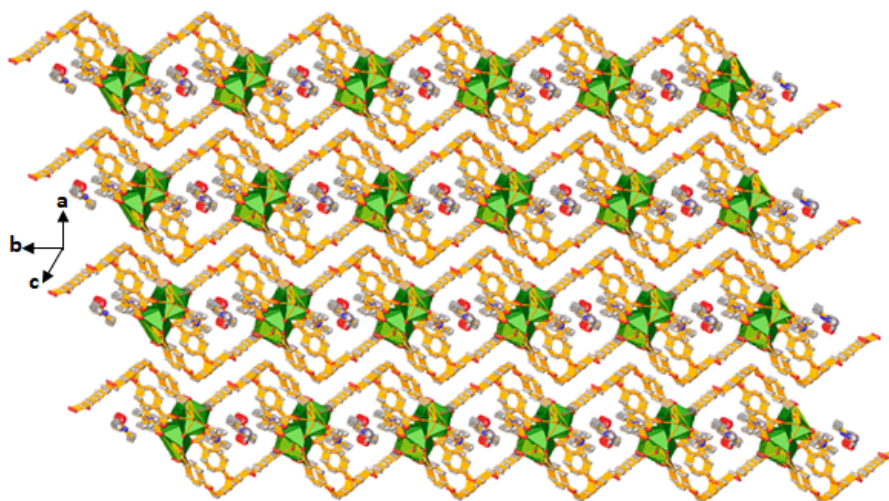


Fig. 6: View of the 3D supramolecular structure of the coordination network EuL along the crystallographic b-axis.

Table 1: Crystal data of the free ligand (H₃L) and the lanthanides-based coordination networks

Compounds	H ₃ L	TbL	GdL	EuL
Emp. Form.	C ₃₀ H ₂₄ O ₉	Tb ₂ C ₆₉ H ₆₇ N ₃ O ₂₃	Gd ₂ C ₆₉ H ₆₇ N ₃ O ₂₃	Eu ₂ C ₆₉ H ₆₇ N ₃ O ₂₃
MW	528.49	1624.09	1620.79	1610.17
T/K	150	150	150	150
λ/Å	Cu Kα	Mo Kα	Mo Kα	Mo Kα
Crystal syst.	Triclinic	Triclinic	Triclinic	Triclinic
Space group	P $\bar{1}$	P $\bar{1}$	P $\bar{1}$	P $\bar{1}$
a/ Å	6.3171(5)	8.5108 (5)	8.5212 (12)	8.5361 (6)
b/ Å	10.6482(7)	14.2208 (9)	14.186 (2)	14.2116(10)
c/ Å	18.1883 (1)	14.3990 (9)	14.434 (2)	14.4375(10)
α/°	86.360 (3)	98.265 (2)	98.010 (3)	98.093 (1)
β/°	88.548 (3)	106.718 (1)	106.609 (3)	106.628 (1)
γ/°	79.326 (3)	96.164 (1)	96.382 (4)	96.329 (1)
V/ Å ³	1199.74 (15)	1631.26 (17)	1634.6 (4)	1640.4 (2)
Z	2	1	1	1
Z'	1	0.5	0.5	0.5
D/Mgm ⁻³	1.463	1.653	1.646	1.630
μ/mm ⁻¹	0.91	2.23	2.10	1.98
F(000)	552	816	814	812
θ range/°	4.2–68.8	2.7–28.2	2.5–28.2	2.7–30.4
^a R ₁ /%	3.19	3.08	2.98	1.70
^b wR ₂ /%	8.60	7.08	6.70	4.61
R _{int} /%	1.51	2.95	5.17	1.51
Goof	1.050	1.054	1.035	1.084

$${}^a R_1 = \frac{\sum(|F_0| - |F_c|)}{\sum|F_0|} \quad {}^b wR_2 = \left\{ \frac{\sum[w(F_0^2 - F_c^2)^2]}{\sum[w(F_0^2)^2]} \right\}^{1/2}$$

The Infrared spectra of the three compounds (Figure S6) exhibit a similar profile with a broad vibrational band in the range of 3000–3500 cm⁻¹ assigned to the vibrations of the coordinated water molecules and the C-H stretching modes of the aromatic ring [44,45]. The weak bands at around 2930 and 2890

cm^{-1} correspond to the symmetric and asymmetric stretching modes of the $-\text{CH}_2-$ groups. The red shift from 1674 to 1650 cm^{-1} of the carbonyl absorption band, comparing to the protonated H_3L , indicates a total deprotonation of the ligand in the CPs, thus in agreement with the single crystal data. The vibration bands of the carboxylate group occur at around 1603 cm^{-1} and at 1407 cm^{-1} attributed to the asymmetric stretching and symmetric stretching, respectively.

In order to check the crystalline phase of the microcrystalline compounds obtained together with mono-crystals, the X-ray powder diffraction (P-XRD) patterns were recorded at room temperature and compared to the simulated ones [46]. As shown in Figure S8 and Figure S9, the peaks positions simulated for EuL and the experimental patterns are in agreement with each other indicating they are isostructural. The difference in reflection intensities between the simulated and experimental patterns is probably due to the variation in preferred orientation of the powder samples during the collection of the experimental P-XRD data.

The thermal stabilities of the compounds were evaluated in the temperature range of 30 to 800°C in a synthetic air atmosphere at a heating rate of 10 °C/min. The thermograms shown in Figure S7 (b-d) exhibit a very similar profile with three weight loss steps beginning at ca. 85, 205 and 325 °C that can be assigned to the loss of lattice solvent molecules, the coordinated ones and the decomposition of the organic part, respectively.

3.3 Electronic properties and photoluminescence study

The absorption spectra recorded in solid state (Figure S4) of the free ligand exhibits an intense band centralized at 248 nm which is bathochromically shifted after coordination to the metal center indicating an extended conjugation probably caused by the metal-perturbed $\pi^*-\pi$ transition of the ligand-centered [47].

In lanthanide complexes, the indirect excitation (called sensitization or antennae effect) of the active ion occurs from an energy migration in terms of the ligand centered absorption followed, mainly, by a singlet to triplet intersystem crossing ($^1\text{S}^* \rightarrow ^3\text{T}^*$) and finally the triplet to lanthanide energy transfer ($^3\text{T}^* \rightarrow \text{Ln}^{\text{III}}$). The efficiency of this complex process involves numerous

rate constants and is highly dependent of the energy gap between the lowest ligand triplet state and the Ln^{III} emitting level [48]. In the cases of Eu^{III} and Tb^{III}, respectively, the triplet ligand state should be localized sufficiently above the ⁵D₀ (17290 cm⁻¹) and ⁵D₄ (20500 cm⁻¹) levels, respectively, allowing efficient energy transfer and prevent quenching via the back-energy transfer [29]. Therefore, it becomes an important issue to determine the triplet state energy of the ligand, which can be calculated by referring to the lower wavelength emission edge of the corresponding phosphorescence spectrum obtained at low temperature of the Gd^{III} complex [49]. When coordinated to the Gd^{III}, the ligand phosphorescence is intensified due to the heavy paramagnetic ion that enhances the intersystem crossing (ISC) from the singlet (¹S) to the triplet (¹T) state because of mixing of the triplet and singlet states assigned to the paramagnetic effect [50,51] and the absence of energy transfer from the ligand to Gd^{III} ion which has the first excited level (⁶P_{7/2}) at 32 200 cm⁻¹ [52]. Therefore, photoluminescence of Gd^{III} complexes involving ligands with aromatic rings is due to electronic transitions between perturbed ligand localized states in the conformation acquired in the crystal structure of this family of compounds [53,54]. Fig. 7 shows the photoluminescence spectra of GdL and of the free ligand for comparison, both upon excitation at 283 nm. The emission spectrum of the free ligand shows the phosphorescence represented by three vibronic bands at 405, 440 and 470 nm but is dominated by the fluorescence band with the maximum at 338 nm (29585 cm⁻¹) owing to the ¹S → ¹S₀ electronic transitions. The assignments of these bands were based on the emission spectrum of the equivalent La^{III} complex shown in Fig. 8. With a delay of 0.05 ms, the two bands at 300 and 354 nm disappear completely indicating that they are owing to allowed singlet to singlet electronic transitions. The more intense phosphorescence band in comparison to fluorescence one can be attributed to the heavy atom effect [55]. After complexation to the Gd^{III}, the fluorescence band is completely attenuated and the vibronic bands are not well defined probably due to the paramagnetic effect that improve the internal conversion and the intersystem crossing [56].

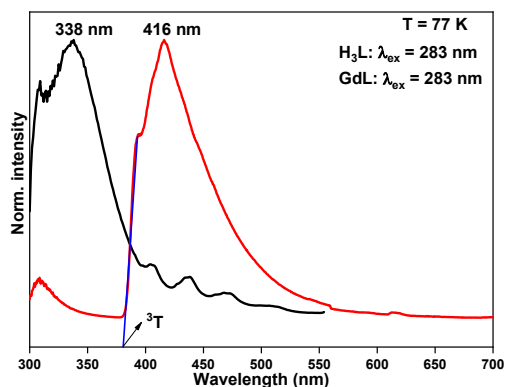


Fig. 7: Emission spectra of the free ligand (Dark) and the gadolinium compound (GdL) (red) at 77 K upon excitation at 283 nm.

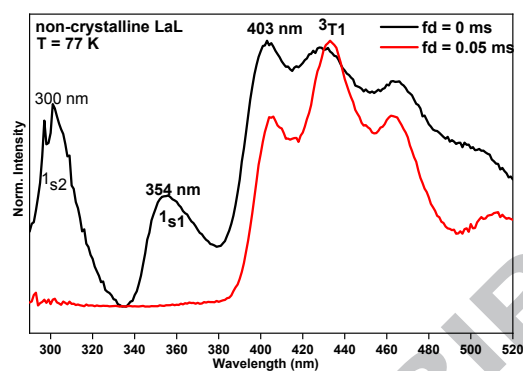


Fig. 8: Stead-state (fd=0ms) (black) and time-resolved (fd=0.05ms) (red) emission of LaL upon excitation at 283 nm at 77 K.

By assuming the shortest phosphorescence band wavelength to be the 0-0 phonon transition (Fig. 7) [57], the triplet state energy was estimated to 26316 cm^{-1} , therefore 9052 and 5816 cm^{-1} above the emitting states of Eu^{III} ($^5\text{D}_0$) and Tb^{III} ($^5\text{D}_4$), respectively. These results suggest that the ligand may sensitize luminescence of both active ions but is more suitable for Tb^{III} . According to the general antennae effect principle, the ligand to metal energy transfer efficiency depends directly on the energy difference between the lowest triplet state level energy of ligands and the emitting level of optically active ion [58].

The solid-state photophysical properties of the compounds EuL and TbL were investigated at three different temperatures. In all cases, the excitation spectra (Fig. 9 and Fig. 15) obtained by monitoring the strongest intensity emission bands, exhibit a broad excitation band with the maximum around 290 nm, which may be attributed to the $\pi^* \leftarrow \pi$ transitions of the benzene rings in the L^3 ligand [45] demonstrating that energy transfer occurs from the ligand to the Eu^{III} and Tb^{III} ions. The excitation spectrum of the EuL coordination network (Fig. 9) shows a series of narrow lines in the longer wavelength region (350 nm to 600 nm) owing to intra-configurational electronic transitions between $^7\text{F}_0$ and $^5\text{L}_6$ electronic states at 393 nm and transitions between $^7\text{F}_{0,1}$ and $^5\text{D}_{2,1}$ levels. The detection of these intra-configurational bands indicates the poor efficiency of the energy transfer from ligand to Eu^{III} . Unexpectedly, the intra-configurational transition becomes more intense at room temperature regarding to the ligand excitation band. This result may suggest an increase of possible

deactivation mechanisms of the singlet state at the expense of the intersystem crossing process.

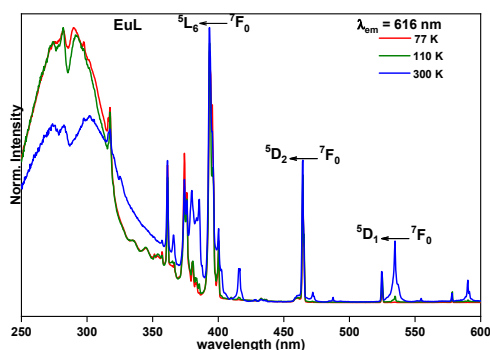


Fig. 9: Normalized excitation spectra obtained at 77 K (red), 110 K (green) and 300 K (blue) of EuL monitoring at 616 nm.

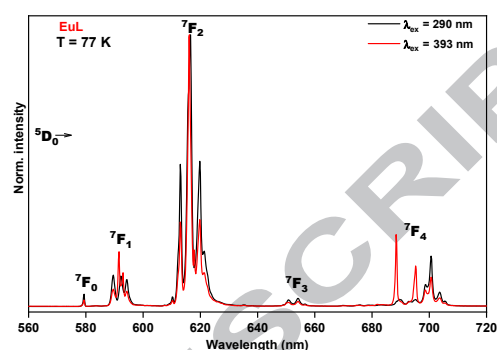


Fig. 10: Normalized emission spectra of EuL obtained at 77 K upon excitation at 290 nm (dark) and at 393 nm (red).

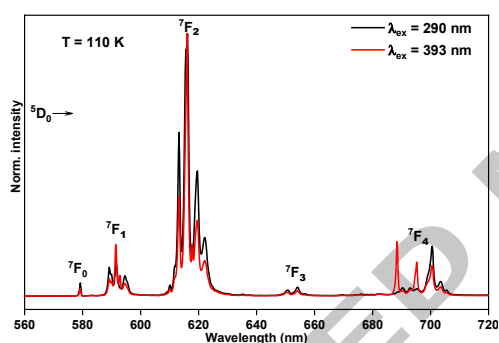


Fig. 11: Normalized emission spectra of EuL obtained at 110 K upon excitation at 290 nm (dark) and at 393 nm (red).

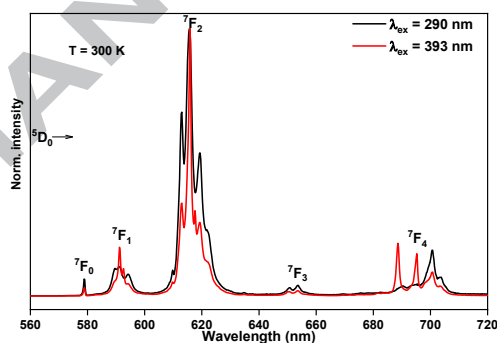


Fig. 12: Normalized emission spectra of EuL obtained at 300 K upon excitation at 290 nm (dark) and at 393 nm (red).

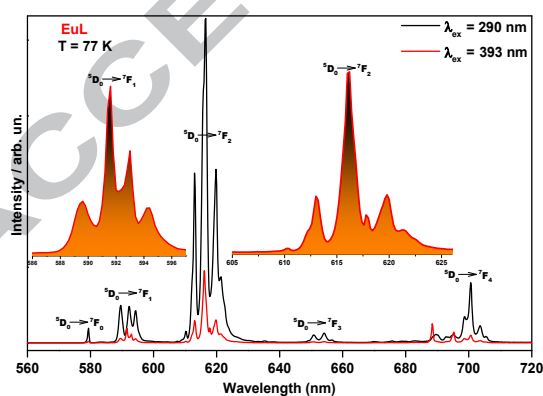


Fig. 13: Emission spectra of EuL at 77 upon excitation at 290 nm and 393 nm. The Insets show the ${}^5D_0 \rightarrow {}^7F_1$ and ${}^5D_0 \rightarrow {}^7F_2$ regions magnified.

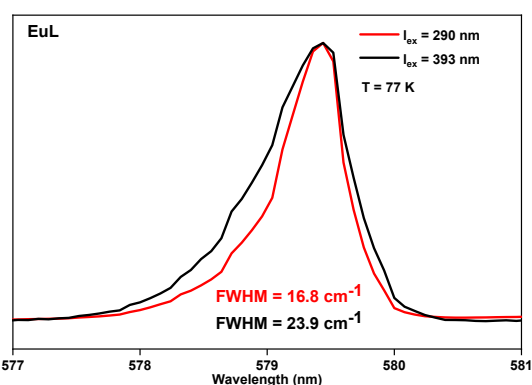


Fig. 14: High resolution ${}^5D_0 \rightarrow {}^7F_0$ emission band of the EuL coordination network obtained at 77 K upon excitation at 290 and 393 nm.

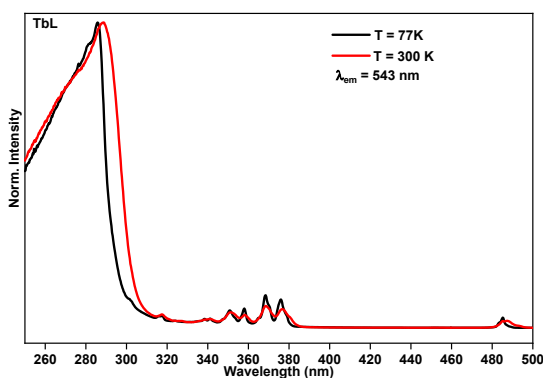


Fig. 15: Excitation spectra obtained at 77 K (dark) and at 300 K (red) of TbL monitoring at 543 nm, normalized with respect to the higher intensity band.

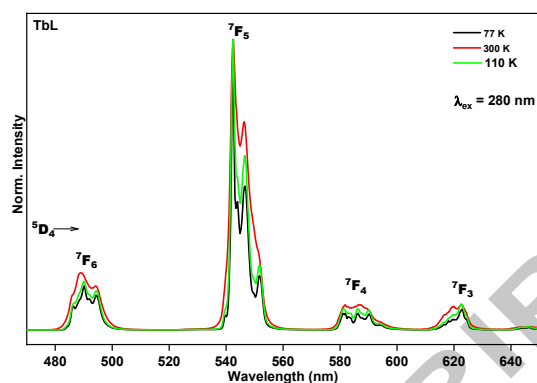


Fig. 16: Emission spectra obtained at 77 K (dark), 110 K (green) and 300 K (red) of TbL upon excitation at 280 nm.

The emission spectra were recorded for all the compounds under ligand excitation and under intra-configurational excitation at 393 nm for EuL (Fig. 10 - Fig. 12 and Fig. 16). EuL and TbL emission spectra show typical Eu^{III} red and Tb^{III} green emissions as narrow and well separated emission bands. For EuL, the well-resolved emission bands are centered at ~579, 592, 616, 651, and 700 nm, corresponding to electronic transitions from the Eu^{III} centered ⁵D₀ excited state to the ⁷F_J (J = 0–4) multiplet ground state with the hypersensitive ⁵D₀→⁷F₂ transition band dominating the spectra, thus in agreement with the fact that the Eu^{III} is located in low-symmetry site without inversion center. The intensity ratio of 8.32 between the ⁵D₀→⁷F₂ forced electric dipole and symmetry sensitive and the ⁵D₀→⁷F₁ magnetic dipole allowed transitions is in good agreement with the low symmetry around the Eu^{III} [21,59]. When excited in the intra-configurational band at 393 nm, the emission bands attributed to ⁵D₀→⁷F₁ and ⁵D₀→⁷F₂ transition are split in four and seven Stark components, respectively (Fig. 13). The resolved emission band attributed to ⁵D₀→⁷F₀ transition remains as an asymmetric and relatively broad one-component band (Fig. 14). A different profile of the emission band attributed to ⁵D₀→⁷F₄ transition is observed when it is compared to the emission spectrum obtained upon excitation at 290 nm. These results suggest an inhomogeneous coordination environment of Eu^{III} ions, which may be assigned to the crystal disorder owing from the two different spatial orientations of the coordinated DMF molecules. Such special orientation probably leads to slight differences around the Eu^{III} sites probably due to small distortions and variations in the Eu-O bond lengths.

Considering the TbL emission spectra, the bands are centered at 489, 542, 586 and 622 nm assigned to the transitions between 5D_4 and 7F_J ($J= 6, 5, 4, 3$) states. The emission lifetimes values were determined, at three different temperatures (77 K, 110 K and 300 K), from the luminescent decay profiles of EuL and TbL by monitoring the most intense emission lines within the $^5D_0 \rightarrow ^7F_2$ and $^5D_4 \rightarrow ^7F_5$ transitions bands, respectively (Fig. 17). The values, depicted in Table 2, were obtained by fitting with mono-exponential functions, indicating that even with the slight differences in symmetry around the ions due to the crystal disorder, in average the emitting states contribute with just one emission lifetime value. This result is corroborated with the $^5D_0 \rightarrow ^7F_0$ band shape obtained at 77K (Fig.14). [27] and it was also observed by Monteiro and co-authors. [60].

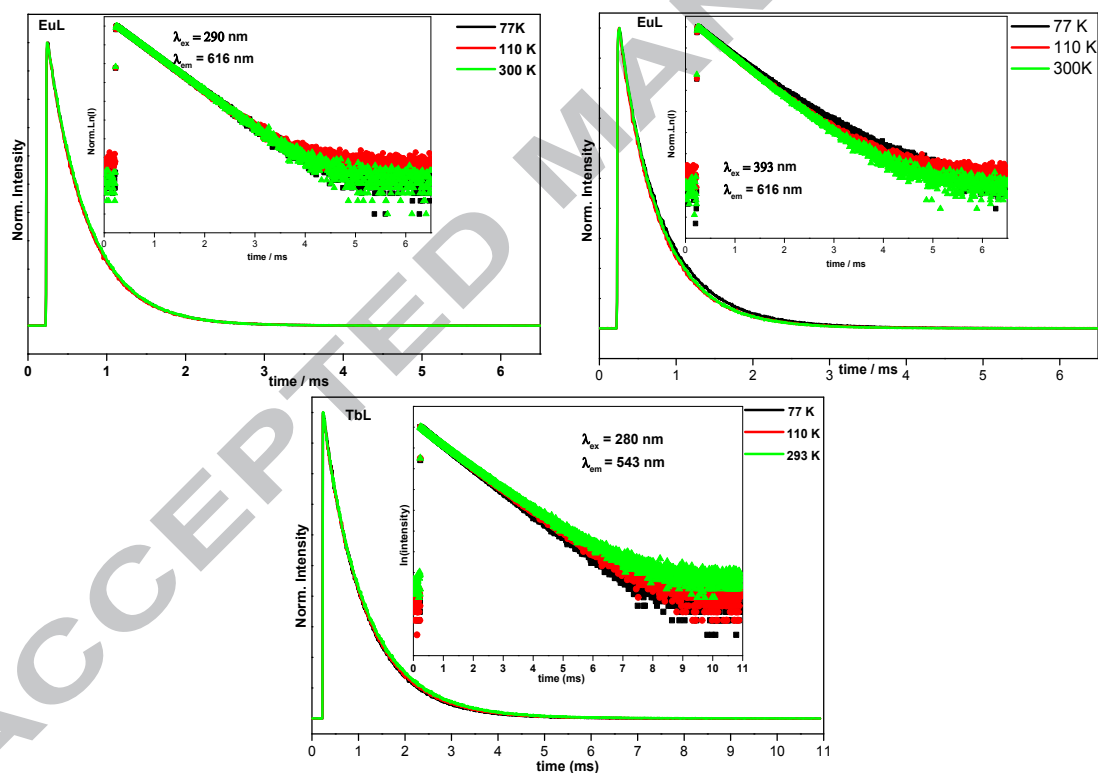


Fig. 17: Experimental luminescence decay curves obtained at 77, 110 and 300 K of the EuL and TbL monitored at 616 nm and 543 nm, respectively, upon excitation at 290 nm and at 393 nm for EuL and 280 nm for TbL.

The observed emission lifetime of EuL and TbL (Fig. 17 and Table 2) obtained in three different temperatures upon excitation in the broad band or at 393 nm

(EuL) remain practically invariable in the temperature range of 77-300 K, indicating a rigid stacking of the crystal lattice.

Table 2: Observed luminescence lifetimes at 77, 110, and 300 K of the coordination networks upon excitation in the ligand for both EuL and TbL and also at 393 for EuL monitoring the emissions at 616 and 543 nm for EuL and TbL, respectively.

	$\lambda_{\text{ex}}/\text{nm}$	$\lambda_{\text{em}}/\text{nm}$	77 K	110 K	300 K
			τ/ms	τ/ms	τ/ms
EuL	290	616	0.507 ± 0.001	0.505 ± 0.002	0.514 ± 0.001
EuL	393	616	0.560 ± 0.004	0.526 ± 0.001	0.530 ± 0.001
TbL	280	543	0.888 ± 0.004	0.907 ± 0.001	0.928 ± 0.008

These slight variations of the emission lifetime values as a function of temperature is probably related to the fact that the efficiency of the ligand to metal energy transfer process is improved as a temperature increases as shown in Figure S11 which shows the emission spectra of GdL at 77 K and 300 K excited in the ligand band. When collected at 77 K, the spectrum shows only the broad band assigned to the ligand owing from the radiative decay of the triplet state, while, at 300 K, the ligand emission is completely attenuated, and narrow emission bands attributed to both Tb^{III} and Eu^{III} were observed due to the presence of Eu^{III} and Tb^{III} as impurities in the compound. As can be seen in Table 2, for the coordination network EuL, the lifetime values obtained exciting at 393 nm are slightly higher than obtained upon excitation in the ligand broad band at 290 nm. The same effect which may be an indication of an increase in the radiative decay rate upon $^5L_6 \leftarrow ^7F_0$ intra-configurational excitation was observed for a Europium coordination framework based on the terephthalic acid [61].

During the last years, many 1D lanthanide coordination networks were reported in the literature. Sheng and co-authors published a series of 1D coordination polymers containing the ions Sm^{III}, Eu^{III}, Tb^{III}, and Dy^{III} based on the 2,4,6-pyridinetricarboxylic acid ligand [62]. Excited at 305nm, all compounds exhibited interesting metal centered luminescence. Using the Schiff-base ligand of N-salicylidenesalicylhydrazide, Feng and co-authors reported a series of Ln-CPs based on the ions Tb^{III}, Dy^{III}, Ho^{III} and Er^{III} with interesting magnetic properties [63]. Recently, Ana and co-authors published a set of eight isolated 1D chains lanthanide networks base on the ligand 3-((anthraquinone-1-

yl)amino)propanoate (aapc) [54]. However, characteristic emission of the Eu^{III} and Tb^{III} , upon excitation in the ligand band, were observed only at low temperature (10 K) even though the lower triplet state level of the ligand aapc (25000 cm^{-1}) comparing to the ligand (H_3L) used in this work (26316 cm^{-1}). In all cases, the compounds showed single molecule magnet behavior making the isolated 1D chain lanthanide coordination network promising for potential applications in quantum-computing devices and molecular spintronics [64]. It worth mention that, despite the large number of Ln-CPs reported until now, to the best of our knowledge, the present work is the first example about the effect of a crystal disorder on the photophysical properties of the trivalent europium ion.

4. Conclusions

In summary, the three dentate 4,4',4''-((Benzene-1,3,5-triyltris(methylene))tris(oxy))tribenzoic acid ligand has been successfully synthesized and used to prepare three new coordination networks containing the Eu^{III} , Tb^{III} and Gd^{III} ions, under solvothermal conditions. Single crystal X-ray and the P-XRD data confirm that the three compounds are isomorphic 1D chain structure. The photoluminescence investigations reveal that both Eu^{III} and Tb^{III} compounds display strong emission bands with lifetimes that slight variates as a temperature function despite presence of solvent molecules in the first coordination sphere of the central ions. Interestingly for the first time, to our knowledge, it is reported a possible effect of crystal disorder of coordination network on the emission profile of the trivalent europium ion.

Acknowledgements

LP is indebted to CNPq (Process: 141691/2015-8) for the Ph.D. fellowship. IOM, ALBF and FAS are indebted to INOMAT (FAPESP: 2014/50906-9), CNPq, CAPES and FAPESP (grant: 2013/22127-2) for financial support. All authors would like to thank the Multiuser Laboratory of Advanced Optical Spectroscopy - Institute of Chemistry-UNICAMP

References

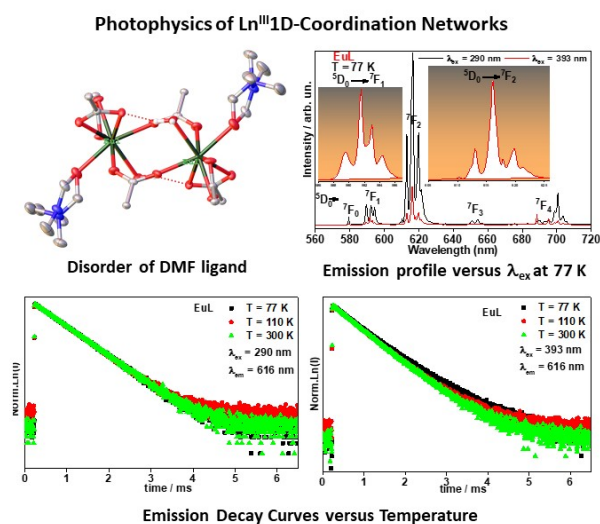
- [1] Y.G. Sun, W. Yu, L. Wang, S.T. Rong, Y.L. Wu, F. Ding, W.Z. Zhang, E.J. Gao, *Inorg. Chem. Comm.* 13 (2010) 479–483. <https://doi.org/10.1016/j.inoche.2010.01.013>

- [2] J.C. Zhang, J.J. Wang, S.L. Zeng, Z.M. Wang, Y. Liu, D.J. Zhang, R.C. Zhang, Y. Fan, *Inorg. Chem. Commun.* 97 (2018) 69–73. <https://doi.org/10.1016/j.inoche.2018.09.021>
- [3] B. Chen, L. Wang, Y. Xiao, F.R. Fronczek, M. Xue, Y. Cui, G. Qian, *Angew. Chem. Int. Ed.* 48 (2009) 500–503. <https://doi.org/10.1002/anie.200805101>
- [4] G.S. Papaefstathiou, L. R. MacGillivray, *Coord. Chem. Rev.* 246 (2003) 169–184. [https://doi.org/10.1016/S0010-8545\(03\)00122-X](https://doi.org/10.1016/S0010-8545(03)00122-X)
- [5] K. Binnemans, R. V. Deun, C. G. Walrand, J.L. Adam, *J. Non. Cryst. Solids.* 238 (1998) 11–29. [https://doi.org/10.1016/S0022-3093\(98\)00540-7](https://doi.org/10.1016/S0022-3093(98)00540-7)
- [6] A. de Bettencourt-Dias, *Dalt. Trans.* (2007) 2229–2241. <https://doi.org/10.1039/b702341c>
- [7] Z. Hu, B.J. Deibert, J. Li. *Chem. Soc. Rev.* 43 (2014) 5815–5840. <https://doi.org/10.1039/c4cs00010b>
- [8] J. Rocha, L.D. Carlos, F.A. A. Paz, D. Ananias, *Chem. Soc. Rev.* 40 (2011) 926–940. <https://doi.org/10.1039/c0cs00130a>
- [9] J. Su, J. Chen, *Lanthanide Metal-Organic Frameworks*, first ed, Tianjin China, 2015. <https://www.springer.com/gp/book/9783662457726>
- [10] L.L. Wu, J. Zhao, H. Wang, J. Wang, *CrystEngComm.* 18 (2016) 4268–4271. <https://doi.org/10.1039/C5CE02444G>
- [11] C. Pagis, M. Ferbinteanu, G. Rothenberg, S. Tanase, *ACS Catal.* 6 (2016) 6063–6072. <https://pubs.acs.org/doi/10.1021/acscatal.6b01935>
- [12] Z.H. Zhang, T. Okamura, Y. Hasegawa, H. Kawaguchi, L.Y. Kong, W.Y. Sun, N. Ueyama, *Inorg. Chem.* 44 (2005) 6219–6227. <https://pubs.acs.org/doi/10.1021/ic050453a>
- [13] M. Wang, X. Meng, F. Song, Y. He, W. Shi, H. Gao, J. Tang, C. Peng, *Chem. Commun.* 2 (2018) 10183–10186. <https://pubs.rsc.org/doi/10.1039/C8CC06058D>
- [14] W. Huang, D. Wu, P. Zhou, W. Yan, D. Guo, C. Duan, Q. Meng, *Cryst. Growth Des.* 9 (2009) 1361–1369. <https://pubs.acs.org/doi/10.1021/cg800531y>
- [15] F.Y. Li, L. Xu, G.G. Gao, L.H. Fan, B. Bi, *Eur. J. Inorg. Chem.* (2007) 3405–3409. <https://doi.org/10.1002/ejic.200601113>
- [16] M. Kumar, M. Kariem, H. N. Sheikh, A. Frontera, S. K. Seth, A. K. Jassal, *Dalt. Trans.* 47 (2018) 12318–12336. <https://pubs.rsc.org/doi/10.1039/c8dt02429d>
- [17] M. Yawer, M. Kariem, P. Sood, H.N. Sheikh, *CrystEngComm.* 18 (2016) 3617–3634. <https://pubs.rsc.org/doi/10.1039/c6ce00321d>
- [18] L. Yang, S. Zhang, X. Qu, Q. Yang, X. Liu, Q. Wei, G. Xie, S. Chen, *J. Solid State Chem.* 231 (2015) 223–229. <http://dx.doi.org/10.1016/j.jssc.2015.08.037>
- [19] J.C.G. Bunzli, S. Comby, A.S. Chauvin, C.D.B. Vandevyver, *J. RARE EARTH.* 25 (2007) 257–274. [https://doi.org/10.1016/S1002-0721\(07\)60420-7](https://doi.org/10.1016/S1002-0721(07)60420-7)
- [20] Y. Cui, F. Zhu, B. Chen, G. Qian, *Chem. Commun.* 51 (2015) 7420–7431. <https://pubs.rsc.org/doi/10.1039/C5CC00718F>
- [21] Z.J. Li, X.Y. Li, Y.T. Yan, L. Hou, W.Y. Zhang, Y.Y. Wang, *Cryst. Growth Des.* 18 (2018) 2031–2039. <https://pubs.acs.org/doi/abs/10.1021/acs.cgd.7b01453>

- [22] Y. Xiao, Y. Cui, Q. Zheng, S. Xiang, G. Qian, B. Chen, *J. Mater. Chem.* 22 (2012) 5503–5505. <https://pubs.rsc.org/doi/10.1039/C0CC00148A>
- [23] X.Z. Song, S.Y. Song, S.N. Zhao, Z.M. Hao, M. Zhu, X. Meng, L.L. Wu, H.J. Zhang, *Adv. Funct. Mater.* 24 (2014) 4034–4041. <https://doi.org/10.1002/adfm.201303986>
- [24] F. Luo, S.R. Batten, *Dalt. Trans.* 39 (2010) 4485–4488. <https://pubs.rsc.org/doi/10.1039/C002822N>
- [25] S. Dang, E. Ma, Z.M. Sun, H. Zhanga, *J. Mater. Chem.* 22 (2012) 16920–16926. <https://pubs.rsc.org/doi/10.1039/c2jm32661b>
- [26] J.K. Molloy, C. Lincheneau, M. M. Karimdjy, F. Agnese, L. Mattera, C. Gateau, P. Reiss, D. Imbert, M. Mazzanti, *Chem. Commun.* 52 (2016) 4577–4580. <https://pubs.rsc.org/doi/10.1039/c6cc01182a>
- [27] D.B.A. Raj, S. Biju, M.L.P. Reddy, *Inorg. Chem.* 47 (2008) 8091–8100. <https://pubs.acs.org/doi/abs/10.1021/ic8004757>
- [28] J.C.G. Bünzli, *Coord. Chem. Rev.* 293 (2015) 19–47. <https://doi.org/10.1016/j.ccr.2014.10.013>
- [29] J.H.S.K. Monteiro, A. de Bettencourt-Dias, F.A. Sigoli, *Inorg. Chem.* 56 (2017) 709–712. <https://pubs.acs.org/doi/abs/10.1021/acs.inorgchem.6b02637>
- [30] H.N. Li, H.Y. Li, L.K. Li, L. Xu, K. Hou, S.Q. Zang, T.C.W. Mak, *Cryst. Growth Des.* 15 (2015) 4331–4340. <https://pubs.acs.org/doi/10.1021/acs.cgd.5b00625>
- [31] M. Kumar, H. N. Sheikh, A. Fraconetti, J.K. Zare, S.C. Sahoo, A. Frontera, *New J. Chem.* 43 (2019) 2179–2195. <https://pubs.rsc.org/doi/10.1039/C8NJ05701J>
- [32] B. Chen, G. Quian, *Metal-Organic Frameworks for Photonics Applications*, New York, USA, 2014. <https://link.springer.com/book/10.1007%2F978-3-642-44967-3>
- [33] P.P. Cui, Y. Zhao, X.D. Zhang, P. Wang, W.Y. Sun, *Dyes and Pigments* 124 (2016) 241–248. <https://doi.org/10.1016/j.dyepig.2015.09.024>
- [34] G.M. Sheldrick, *Acta Cryst. A* 64 (2008) 112–122. <https://doi.org/10.1107/S0108767307043930>
- [35] C.F. Macrae, P.R. Edgington, P. McCabe, E. Pidcock, G.P. Shields, R. Taylor, M. Towler, J. v. de Streek, *J. Appl. Crystallogr.* 39 (2006) 453–457. <https://doi.org/10.1107/S002188980600731X>
- [36] H. Wang, D. Zhao, Y. Cui, Y. Yang, G. Qian, *J. Solid State Chem.* 246 (2017) 341–345. <https://doi.org/10.1016/j.jssc.2016.12.003>
- [37] S. Förster, W. Seichter, E. Weber, *Z. Naturforsch.* 66b (2011) 939 – 946. <https://doi.org/10.1515/znb-2011-0912>
- [38] J.P. Perdew, M. Ernzerhof, *J. Chem. Phys.* 105 (2010) 9982–9985. <https://doi.org/10.1063/1.472933>
- [39] C. Adamo, V. Barone *J. Chem. Phys.* 110 (1999) 6158–6170. <https://doi.org/10.1063/1.478522>
- [40] F. Weigenda, R. Ahlrichsb, *Chem. Phys.* 7 (2005) 3297–3305. <https://pubs.rsc.org/doi/10.1039/B508541A>
- [41] G.L. Stoychev, A.A. Auer, F. Neese, *J. Chem. Theory Comput.* 13 (2017) 554–562. <https://pubs.acs.org/doi/10.1021/acs.jctc.6b01041>

- [42] F. Neese, *Comput. Mol. Sci.* 2 (2012) 73–78. <https://doi.org/10.1002/wcms.81>
- [43] O. Karagiari, W. Bury, A.A. Sarjeant, J.T. Hupp, O.K. Farha, *J. Vis. Exp.* (2014) 1–9. <http://www.doi.org/10.3791/52094>
- [44] R. Ilmi, K. Iftikhar, *Polyhedron*. 102 (2015) 16–26. <https://doi.org/10.1016/j.poly.2015.07.046>
- [45] S.J. Wang, H.L. Wu, L.X. You, G. Xiong, Y.K. He, F. Ding, Y.G. Sun, *Inorg. Chim. Acta*. 485 (2019) 49–53. <https://doi.org/10.1016/j.ica.2018.09.083>
- [46] J. Rong, W. Zhang, J. Bai, *CrystEngComm*. 18 (2016) 7728–7736. <https://pubs.rsc.org/doi/10.1039/C6CE01585A>
- [47] M. H. V. Werts, M. A. Duin, J.W. Hofstraat, J. W. Verhoeven, *chem. comm.* (1999) 799–800. <https://pubs.rsc.org/doi/10.1039/A902035G>
- [48] A. Beeby, S. Faulkner, D. Parkera, J.A.G. Williams, *J. Chem. Soc. Perkin Trans. 2*. 0 (2001) 1268–1273. <https://pubs.rsc.org/doi/10.1039/B009624P>
- [49] B. Yan, H. Zhang, S. Wang, J. Ni, *J. Photochem. Photobiol. A Chem.* 116 (1998) 209–214. [https://doi.org/10.1016/S1010-6030\(98\)00307-4](https://doi.org/10.1016/S1010-6030(98)00307-4)
- [50] Y.L. Gai, F.L. Jiang, L. Chen, Y. Bu, K.Z. Su, S.A. A. Thabaiti, M.C. Hong, *Inorg. Chem.* 52 (2013) 7658–7665. <https://pubs.acs.org/doi/10.1021/ic400777c>
- [51] M. Kleinerman, *J. Chem. Phys.* 51 (1969) 2370. <http://dx.doi.org/10.1063/1.1672355>
- [52] W.T. Carnall, H. Crosswhite, H.M. Crosswhite, *Energy level structure and transition probabilities in the spectra of the trivalent lanthanides in LaF₃*, United States, 1978. <https://www.osti.gov/biblio/6417825/>
- [53] A.I. Baba, J.R. Shaw, J.A. Simon, R.P. Thummel, R.H. Schmehl, *Coord. Chem. Rev.* 171 (1998) 43–59. [https://doi.org/10.1016/S0010-8545\(98\)90009-1](https://doi.org/10.1016/S0010-8545(98)90009-1)
- [54] A. B.R. Muelle, A. G. García, A.A. G. Valdivia, I. Oyarzabal, J. Cepeda, J.M. Seco, E. Colacio, A.R. Diéguez, I. Fernández, *Dalt. Trans.* 47 (2018) 12783–12794. <https://pubs.rsc.org/doi/10.1039/c8dt02592d>
- [55] H. Xu, R. Chen, Q. Sun, W. Lai, Q. Su, W. Huang, X. Liu, *Chem. Soc. Rev.* 43 (2014) 3259–302. <https://pubs.rsc.org/doi/10.1039/c3cs60449g>
- [56] S. Tobita, M. Arakawa, I. Tanaka, *J. Phys. Chem.* 89 (1985) 5649–5654. <https://pubs.acs.org/doi/abs/10.1021/j100272a015>
- [57] J.H.S.K. Monteiro, A. De Bettencourt-Dias, I.O. Mazali, F.A. Sigoli, *New J. Chem.* 39 (2015) 1883–1891. <https://pubs.rsc.org/doi/10.1039/C4NJ01701C>
- [58] B. Yan, H.J. Zhang, S.B. Wang, J.Z. Ni, *Monatshette Für Chemie*. 129 (1998) 151–158. <https://doi.org/10.1007/PL00010151>
- [59] F.F. Chen, Z.Q. Bian, Z.W. Liu, D.B. Nie, Z.Q. Chen, C.H. Huang, *Inorg. Chem.* 47 (2008) 2507–2513. <https://pubs.acs.org/doi/10.1021/ic701817n>
- [60] J.H.S.K. Monteiro, J.D. L. Dutra, R.O. Freire, A.L.B. Formiga, I.O. Mazali, A. de Bettencourt-Dias, F.A. Sigoli, *Inorg. Chem.* 57 (2018) 15421–15429. <https://pubs.acs.org/doi/10.1021/acs.inorgchem.8b02720>
- [61] J.F.S. do Nascimento, B.S. Barros, J. Kulesza, J.B.L. de Oliveira, A.K.P. Leite, R.S. de Oliveira, *Mater. Chem. Phys.* 190 (2017) 166–174. <https://doi.org/10.1016/j.matchemphys.2017.01.024>

- [62] Y. Huang, Y.S. Song, B. Yan, M. Shao, J. Solid State Chem. 181 (2008) 1731–1737. <https://doi.org/10.1016/j.jssc.2008.03.036>
- [63] H.K. Feng, P.J. Huang, H.L. Tsai, Dalt. Trans. 44 (2015) 3764–3772. <https://pubs.rsc.org/doi/10.1039/c4dt03458a>
- [64] J.G. Segura, J. Veciana, D. R. Molina, Chem. Commun. (2007) 3699–3707. <https://pubs.rsc.org/doi/10.1039/B616352A>



Highlights

Photophysics of Eu^{III} and Tb^{III} 1D-coordination networks

Static crystal disorder due to the different spatial orientations of DMF molecules

Influence of DMF orientations on Eu^{III} chemical environments and emission Stark sublevels

Eu^{III} emission lifetime invariability as function of temperature